Substitutions that lock and unlock the proton-coupled folate transporter (PCFT-SLC46A1) in an inward-open conformation

Received for publication, August 23, 2018, and in revised form, March 6, 2019 Published, Papers in Press, March 11, 2019, DOI 10.1074/jbc.RA118.005533

Srinivas Aluri[‡], Rongbao Zhao[‡§], Kai Lin[‡¶], Daniel Sanghoon Shin[‡§1], Andras Fiser[‖], and I. David Goldman[‡§2]**

*From the Departments of [‡]Pharmacology, [§]Medicine, [‖]Systems and Computational Biology, and **Biochemistry, Albert Einstein College of Medicine, Bronx, New York 10461 and the [¶]Air Force Medical Center, PLA, Beijing 100142, China*

Edited by Mike Shipston

The proton-coupled folate transporter (PCFT) mediates intestinal absorption of folates and their transport from blood to cerebrospinal fluid across the choroid plexus. Substitutions at Asp-109 in the first intracellular loop between the first and second transmembrane domains (TMDs) abolish PCFT function, but protein expression and trafficking to the cell membrane are retained. Here, we used site-directed mutagenesis, the substituted-cysteine accessibility method, functional analyses, and homology modeling to determine whether the D109A substitution locks PCFT in one of its conformational states. Cys-substituted residues lining the PCFT aqueous translocation pathway and accessible in WT PCFT to the membrane-impermeable cysteine-biotinylation reagent, MTSEA-biotin, lost accessibility when introduced into the D109A scaffold. Substitutions at Gly-305 located exofacially within the eighth TMD, particularly with bulky residues, when introduced into the D109A scaffold largely restored function and MTSEA-biotin accessibility to Cys-substituted residues within the pathway. Likewise, Ser-196 substitution in the fifth TMD, predicted by homology modeling to be in proximity to Gly-305, also partially restored function found in solute transporters, is critical to oscillation of the carrier among its conformational states. Substitutions at Asp-109 and Gly-112 lock PCFT in an inward-open conformation, resulting in the loss of function. However, the integrity of the locked protein is preserved, indicated by the restoration of function after insertion of a second "unlocking" mutation. and accessibility. Similarly, the inactivating G112K substitution within the first intracellular loop was partially reactivated by introducing the G305L substitution. These data indicate that the first intracellular loop, with a sequence identical to "motif A" (G*XXX*D*XX*GR(R/K))

The proton-coupled folate transporter (PCFT)[3] is required for the intestinal absorption of folates and folate transport from blood to cerebrospinal fluid across the choroid plexus. Mutations in the PCFT gene that result in loss of function of the protein lead to the autosomal recessive disorder, hereditary folate malabsorption (HFM), in which there is impaired or complete loss of function of both processes (1–3). This transporter also has a high affinity for certain antifolates, in particular (i) pemetrexed, an inhibitor of thymidylate and purine synthesis (4), and (ii) new generation inhibitors of glycinamide ribonucleotide transformylase, all agents that inhibit their target enzymes after polyglutamation within cancer cells (5). Because of its low pH optimum, PCFT is active within the acidic tumor microenvironment (4). This is unlike the reduced folate carrier (RFC), with a pH optimum of 7.4, that delivers folates and antifolates into systemic tissues within their physiological milieu (1, 3, 6). Recent studies point to the important role PCFT, in contrast to RFC, plays in the efficacy of pemetrexed in the treatment of pleural mesothelioma (7).

Since the discovery of PCFT (2), there have been extensive studies employing site-directed mutagenesis that have defined the topology of this transporter and identified residues and regions that play a critical role in its function (1). Among these are residues critical to proton coupling (8), proton binding (9), and helices that contribute to a gate at the exofacial boundary of the carrier (10). These studies have been complemented by analyses of the causative mutations detected in subjects with HFM. Whereas the majority of these mutations result in the loss of PCFT protein, in a few cases, sufficient expression and function is preserved to allow characterization of the transport defect (11–13).

Of all of the reported mutant forms of PCFT that were expressed but lost function, only one residue has been identified that is absolutely required for function irrespective of the substituting residue: Asp-109, located in the first intracellular loop bounded by the second and third transmembrane domains (TMDs) (14). Further evidence for the importance of this region of the protein were observations that there is also a profound loss of function with mutations of two additional residues in this loop, Gly-112 and Arg-113, the latter a site of mutation in two subjects with HFM (15–17). These three residues are fully conserved across species. The sequence of this loop conforms to the conserved motif A (G*XXX*D*XX*GR(R/K))

This work was supported by NCI, National Institutes of Health, Grant CA082621. The authors declare that they have no conflicts of interest with the contents of this article. The content is solely the responsibility of the authors and does not necessarily represent the official views of the National Institutes of Health.

[1] Present address: Division of Hematology-Oncology, Dept. of Medicine, UCLA, Los Angeles, CA 90095.

[2] To whom correspondence should be addressed: Albert Einstein College of Medicine, 1300 Morris Park Ave., Bronx, NY 10461. Tel.: 718-430-2302; Fax: 718-430-8550; E-mail: i.david.goldman@einstein.yu.edu.

[3] The abbreviations used are: PCFT, proton-coupled folate transporter; TMD, transmembrane domain; RFC, reduced folate carrier; MTX, methotrexate; HFM, hereditary folate malabsorption; MFS, major facilitator superfamily; ANOVA, analysis of variance; MTSEA, 2-aminoethyl methanethiosulfonate; ATB-BMPA, 2-*N*-4-(1-azi-2,2,2-trifluoroethyl)benzoyl-1,3-bis-(D-mannos-4-yloxy)-2-propylamine.

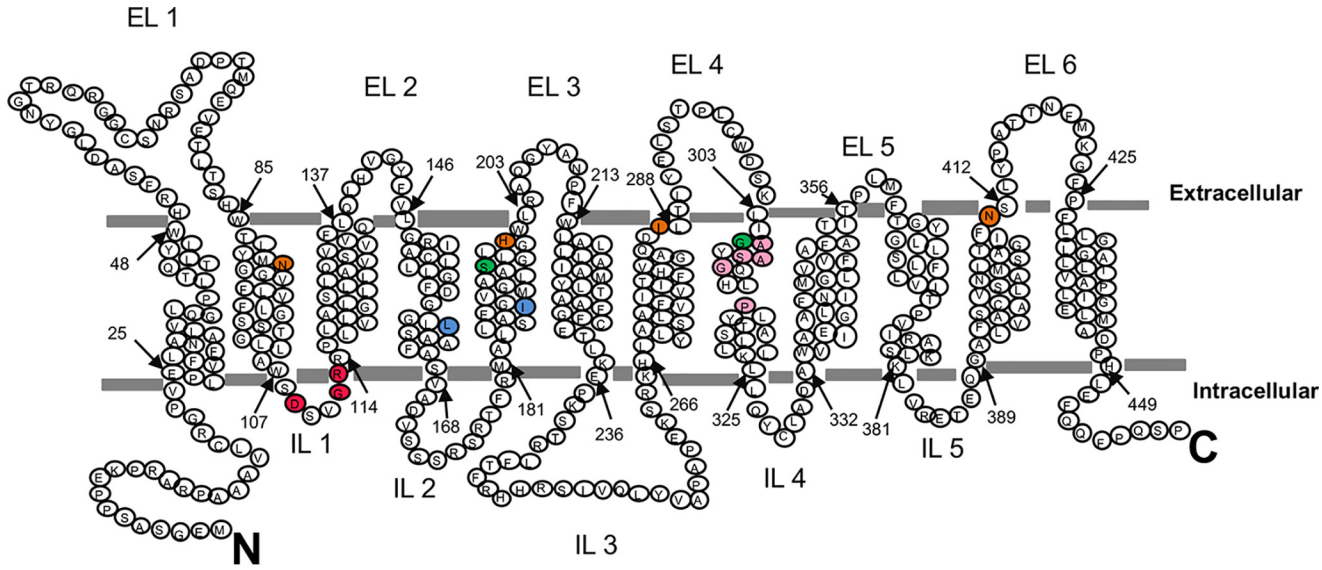

Figure 1. Topological structure of PCFT. The secondary structure of PCFT consists of 12 transmembrane domains with N and C termini directed to the cytoplasm (22). Residues in the first intracellular loop (Asp-109, Gly-112, and Arg-113) are *highlighted* in *red*. Cys-substituted residues studied, that are accessible in PCFT-WT, are *highlighted* in *orange*. Two residues that when mutated restore function when introduced in the D109A scaffold are *highlighted* in *green* (Gly-305 (eighth TMD) and Ser-196 (fifth TMD)). Cys-substituted residues studied in the eighth TMD are indicated in *pink*. Ile-188 (fifth TMD) and Leu-161 (fourth TMD) are *highlighted* in *blue*. The *arrows* indicate the positions of amino acids predicted to be located at membrane interfaces.

which plays a major role in the function of the major facilitator superfamily (MFS) of solute transporters (18, 19).

The degree to which function was lost with mutations at the Asp-109 residue raised the possibility that alterations at this site might lock the protein in one of its conformational states. This possibility is the subject of the current study with a focus on alterations in accessibility of Cys-substituted residues in the D109A scaffold that are accessible to MTSEA-biotin in WT PCFT (PCFT-WT). The data obtained are consistent with the formation of a protein locked in its inward-open conformation when Asp-109 is mutated, indicating that the integrity of this loop, and this residue in particular, is an essential requirement for carrier function. Second mutations in remote exofacial regions of the protein were also identified that, when inserted in the D109A scaffold, restored both transport activity and accessibility of Cys-substituted residues within the aqueous translocation pathway.

Results

The impact of an inactivating D109A mutation on the extracellular accessibility of Cys-substituted PCFT residues

Asp-109 is located in the first intracellular loop of PCFT between the second and third TMDs (Fig. 1). This laboratory previously reported that substitution of Asp-109 with a variety of other residues resulted in a complete loss of function but did not alter the level of PCFT protein expressed or that trafficked to the cell membrane (14). This is unlike the majority of other PCFT mutants studied, where this degree of loss of function was usually due to instability and loss of the protein (1, 14, 15). Likewise, mutations at two other conserved residues in this loop, Arg-113 (15, 16) and Gly-112 (17), also result in a marked loss of activity consistent with an important role for this loop in PCFT function. The loss of function of Asp-109 mutants was so profound that it raised the possibility that mutations at this residue might lock the protein in one of its conformational states. To assess this possibility, the accessibility of Cys-substituted PCFT mutants, previously shown to be accessible from the extracellular compartment in the PCFT-WT (L161C and I188C, fourth and fifth TMDs, respectively, indicated in *blue* in Fig. 1) (20, 21), was evaluated. These Cys-substituted mutations were inserted into the D109A scaffold, and their surface expression and accessibility to the membrane-impermeant MTSEA-biotin were evaluated.

There was robust surface expression of all of the single and double mutants in the crude membrane extract and at the cell surface (Fig. 2*A*). However, the accessibility of the Cys-substituted, D109A double mutants was lost when probed with MTSEA-biotin, whereas all of the individual Cys-substituted mutants were accessible. None of the endogenous Cys residues in PCFT-WT or the D109A scaffold were accessible to MTSEA-biotin as reported previously (22). Hence, the D109A mutation resulted in the loss of accessibility of the two Cys-substituted mutants (L161C/D109A and I188C/D109A) to the extracellular compartment. To determine the effect of these mutations on transport activity, [^{3}H]methotrexate (MTX) influx was assessed at a concentration far below the influx K_t (0.5 μM) and at a saturating concentration (50 μM). It can be seen in Fig. 2*B* that each of the single Cys-substituted mutants was active; indeed, activity of the I188C-PCFT was much greater than that of PCFT-WT. The marked increase at the high MTX concentration accompanied by little change at the low concentration was consistent with both an increased K_t and V_{max} because an increase in the latter should produce a comparable proportional increase in rate irrespective of the substrate concentration, as reported for a variety of mutations at other residues (23–25). Despite this, the I188C/D109A and L161C/D109A double mutants lost all function.

To more broadly explore the impact of the D109A mutation, additional Cys-substituted residues were studied that are located at the exofacial membrane interface and are accessible

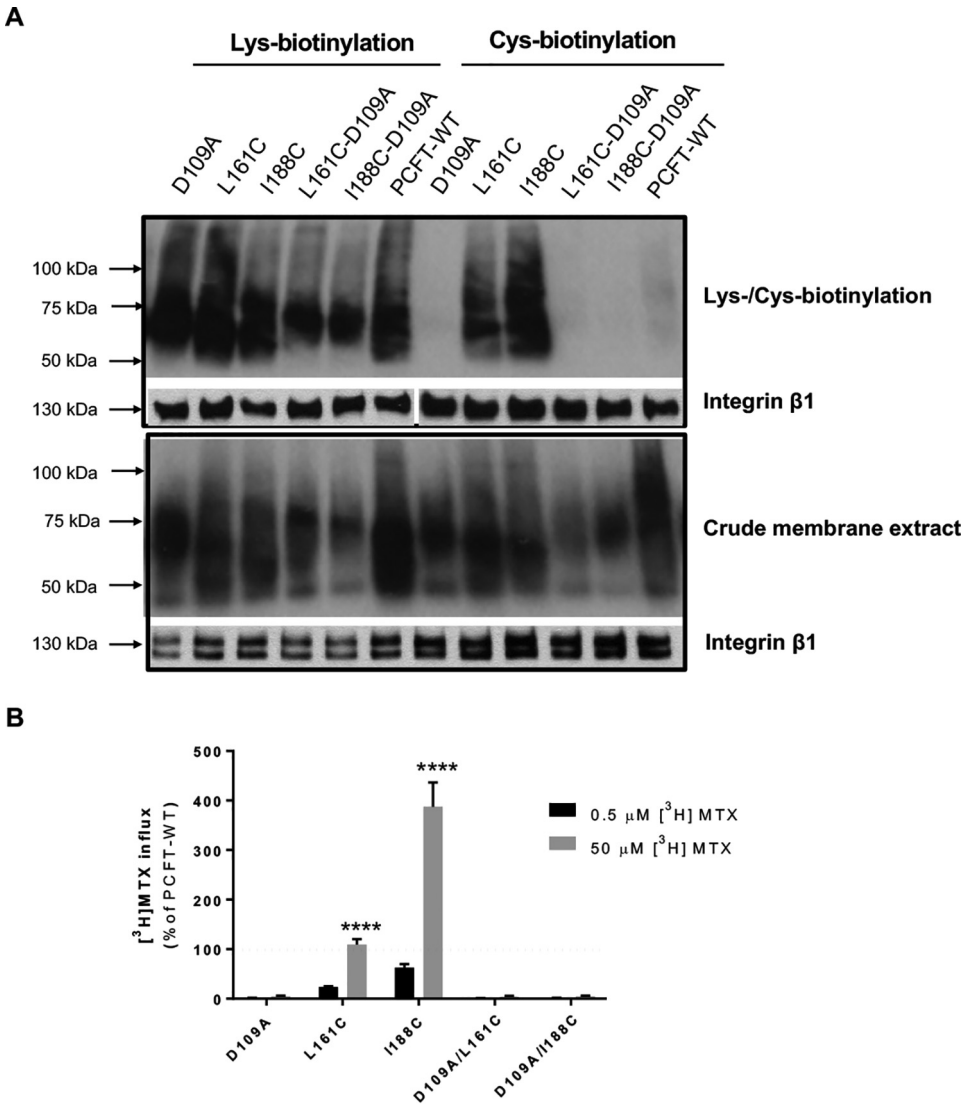

Figure 2. The impact of the D109A mutation on the accessibility and function of Cys-substituted mutants. *A,* in this Western blotting, the *top row* indicates Lys biotinylation at the cell membrane (*left*) and Cys biotinylation (*right*) of mutants and WT. The *bottom row* indicates total PCFT expression in the corresponding crude membrane extracts. Integrin β1 is the loading control for both biotinylated and crude membrane proteins. The *gap* between integrin β1 loading controls for Lys biotinylation and Cys biotinylation indicates different exposure times of the X-ray films. The Western blotting is representative of three independent experiments. *B,* [^{3}H]MTX influx was assessed at 37 °C and pH 5.5 over 1 min at concentrations of 0.5 μM (an order of magnitude below the MTX influx K_t) and 50 μM (an order of magnitude above). Data are indicated as percentage $\pm$ S.E. (*error bars*) of PCFT-WT influx from three independent experiments. A one-way ANOVA compared single Cys mutants with corresponding D109A double mutants. ****, $p < 0.0001$.

to MTSEA-biotin in PCFT-WT. These included, as indicated in *orange* in Fig. 1, H201C (fifth TMD), I287C (seventh TMD), and two residues previously reported to be located within the PCFT extracellular gate, N90C (second TMD) and N411C (eleventh TMD) (10). It can be seen in Fig. 3*A* that each of the individual Cys-substituted mutants is expressed (*bottom row*), traffics to the cell membrane (*middle row*), and is accessible to MTSEA-biotin (*top row*). Of the four double mutants expressed at the cell membrane, only the H201C/D109A mutant remained accessible to the probe, likely related to its more extracellular orientation. Hence, the change in the protein conformation induced by the D109A mutation excluded most but not all of the residues at the exofacial interface that were evaluated. [^{3}H]MTX influx was assessed for all of the mutants (Fig. 3*B*). There was a modest reduction in transport activities for the N90C and N411C and, to a lesser extent, for the H201C mutants. There was a modest increase in transport mediated by the I287C mutant at the saturating concentration with no change at the lower concentration, again consistent with a modest increase in both the influx K_t and V_{max}. In all cases, influx was abolished for the mutants harboring the D109A mutation at low and high MTX concentrations.

Analysis of the pattern of accessibility of Cys-substituted residues in the eighth TMD, a component of a deep exofacial cleft within the plasma membrane

Previous studies demonstrated that 14 consecutive Cys-substituted exofacial residues of the 23 residues in the eighth TMD are accessible to MTSEA-biotin, as are 9 of 23 Cys-substituted exofacial residues of the seventh TMD. This suggested that these two exofacial helices are part of a deep exofacial cleft in the membrane (23, 25). To determine how this pattern of acces-

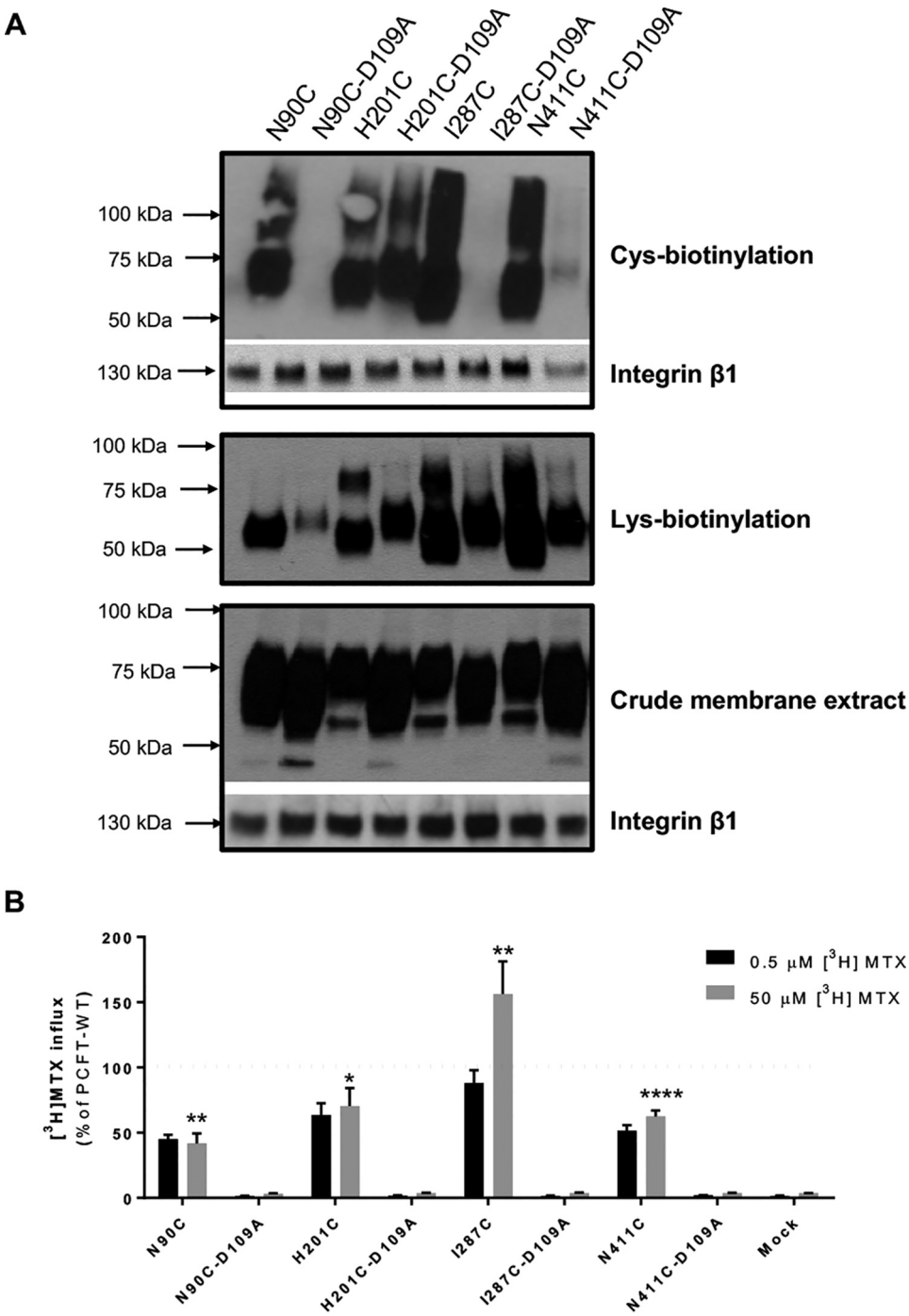

Figure 3. The impact of the D109A mutation on the accessibility of Cys-substituted exofacial residues within TMDs and including the region of the external gate. *A*, MTSEA-biotin accessibility of Cys-substituted residues with the integrin β1 loading control is shown in the *top row*, whereas surface expression of the mutants is indicated in the *middle row*. PCFT expression in the crude membrane extracts is indicated in the *bottom row* with the integrin β1 loading control. The Western blotting is a representative of three independent experiments. *B*, [^{3}H]MTX influx was assessed at 37 °C and pH 5.5 over 1 min at concentrations of 0.5 and 50 μM. Data are represented as percentage $\pm$ S.E. (*error bars*) of PCFT-WT influx from three independent experiments. A one-way ANOVA compared single mutant with each double mutant. *, $p < 0.05$; **, $p < 0.01$; ****, $p < 0.0001$.

sibility might change when the D109A mutation was introduced, Cys-substituted residues were singly and sequentially inserted into the D109A scaffold and then probed with MTSEA-biotin. As indicated in the *middle panel* of Fig. 4*A*, all of the mutants were expressed at the cell membrane, although the level of expression of some double mutants was modestly lower than that of the corresponding single mutants. There was retarded migration of all double mutants relative to the single mutants, as also observed in Fig. 3*A*; the basis for this was not clear. As indicated in the *top row*, accessibility to MTSEA-biotin was retained for the G305C/D109A and, to a lesser extent, for the G307C/D109A and S308C/D109A mutants located proximal to the exofacial membrane boundary. However, the accessibility of the Cys-substituted residues deeper in the eighth TMD was lost (A309C/D109A, A310C/D109A, and P314C/D109A) although the expression of the mutants on the

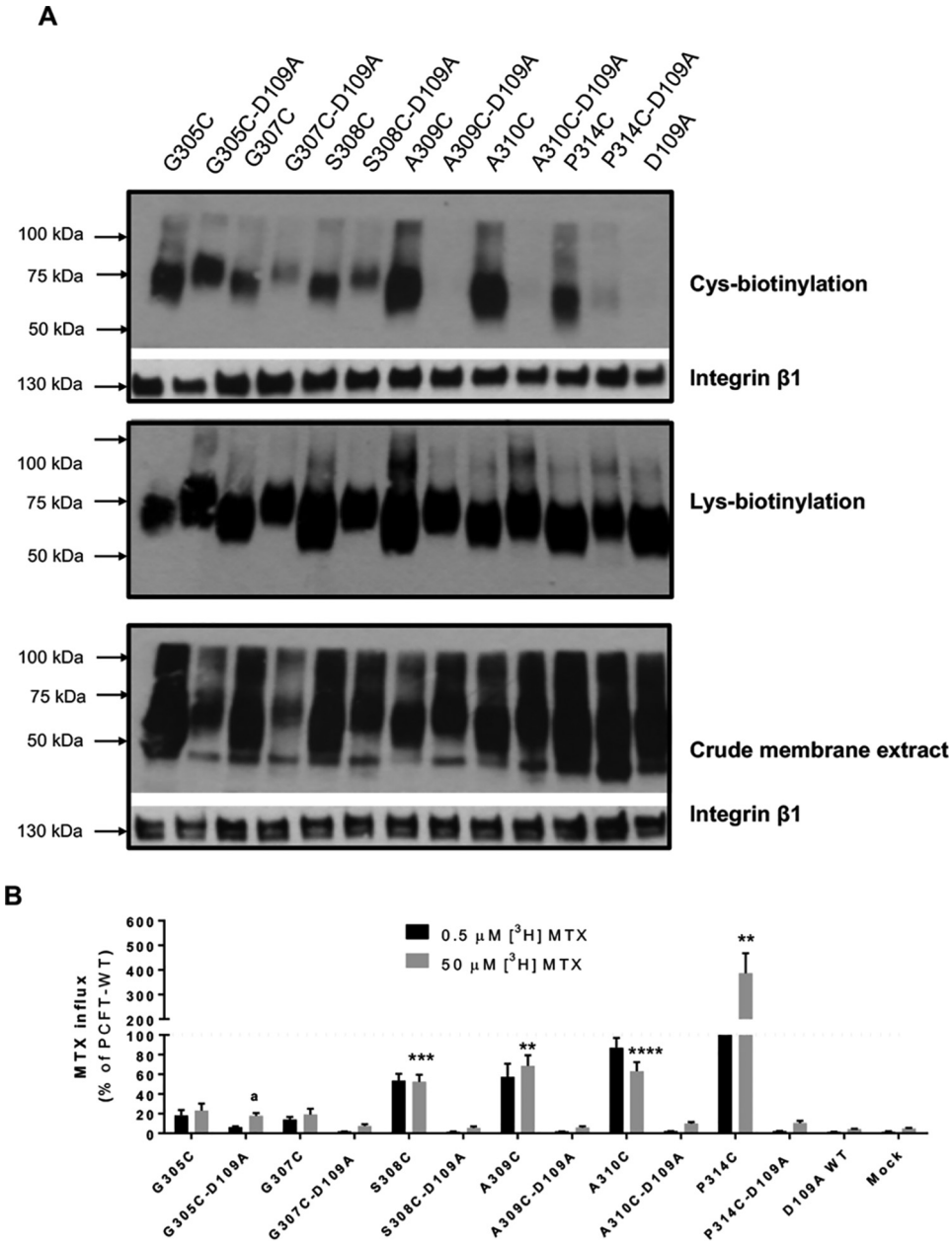

Figure 4. The impact of the D109A mutation on accessibility to MTSEA-biotin of resides within the exofacial cleft of the eighth TMD. *A*, in the *top* row, the accessibility of Cys-substituted residues to MTSEA-biotin of the single mutants, or in combination with the D109A mutation, are shown going from *left* to *right* in the figure from a residue (G305C) high in the exofacial region to a residue (P314C) deep within the aqueous pathway. Integrin β1 is the loading control. The *middle row* indicates expression at the plasma membrane. The *bottom row* indicates PCFT expression in the crude membrane extract with the integrin β1 loading control. The Western blotting is a representative of three independent experiments. *B*, [^{3}H]MTX influx was assessed at 37 °C and pH 5.5 over 1 min at concentrations of 0.5 and 50 μM. Data are represented as percentage $\pm$ S.E. (*error bars*) of PCFT-WT influx from three independent experiments. A one-way ANOVA compared single mutant with each double mutant. *, $p < 0.05$; **, $p < 0.01$; ***, $p < 0.005$; ****, $p < 0.0001$. An ANOVA of G305C/D109A *versus* D109A or mock at the high concentration ($p < 0.05$) is indicated as *a*.

plasma membrane was robust. On the other hand, accessibility of the I287C/D109A mutant at the exofacial boundary of the seventh TMD was lost (Fig. 3*A*). Hence, the D109A mutation markedly occluded the aqueous pathway within this exofacial cleft although at different levels for the two helices.

Of particular interest were the findings obtained when the impact of these double mutations on PCFT function was assessed. As illustrated in Fig. 4*B*, the D109A double mutants from G307C to P314C lost all function despite the fact that the activity of the latter mutant was markedly increased consistent with a 3-fold increase in influx V_{max}, as observed previously (23, 24). However, introduction of the G305C mutation into the D109A scaffold produced a very small but significant restoration of function ($p < 0.05$). Studies were then undertaken to determine whether the nature of the substitution at the Gly-305 residue might impact the degree of restoration of D109A activity.

Structural requirements at the Gly-305 residue for restoration of D109A function

A variety of Gly-305 mutations were introduced into the D109A PCFT scaffold to determine whether activation

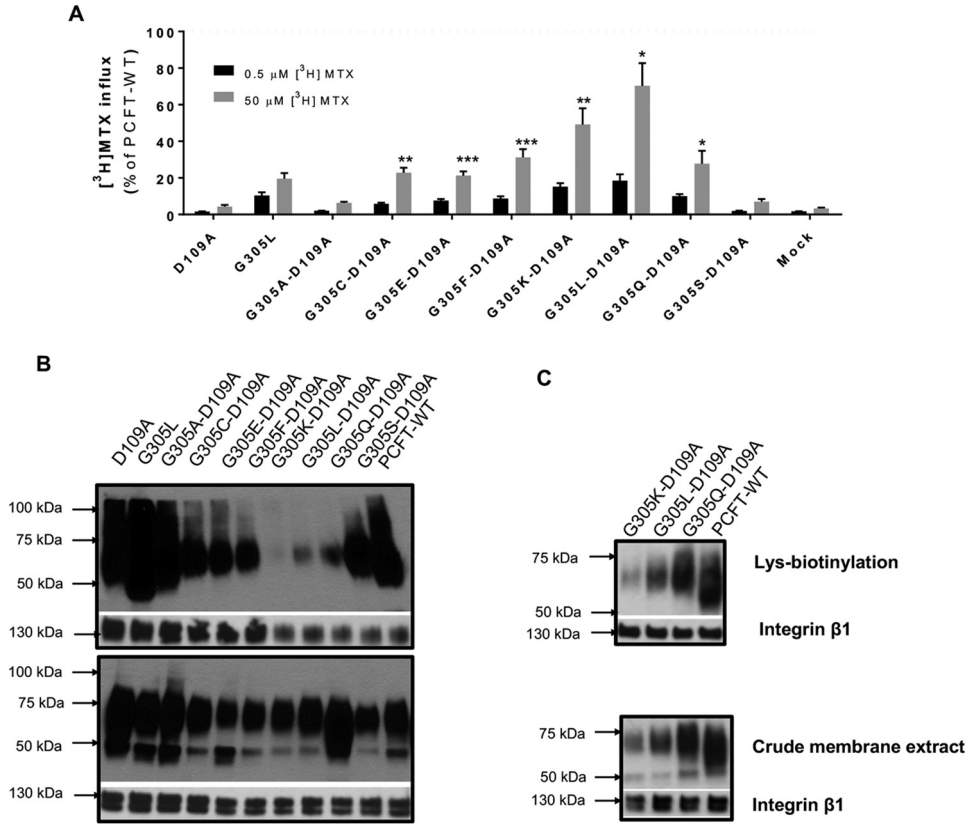

Figure 5. Structural requirements at the Gly-305 position for restoration of D109A function. *A*, [^{3}H]MTX influx was assessed for the D109A mutant alone and in combination with a variety of substitutions at the Gly-305 residue. Uptake was assessed for 1 min at 37 °C at pH 5.5 at MTX concentrations of 0.5 and 50 μM. Data are represented as percentage ± S.E. (*error bars*) of PCFT-WT from three independent experiments. A one-way ANOVA compared D109A with each Gly-305 double mutant. *, $p < 0.05$; **, $p < 0.01$; ***, $p < 0.005$. *B*, expression of mutants at the cell membrane measured by the Lys biotinylation reagent, EZ-link Sulfo-NHS-LC-Biotin. The *top row* indicates PCFT expression at the cell surface, and the *bottom row* indicates expression in the crude membrane extract, each with integrin β1 as the loading control. *C*, surface expression of selective mutants measured by the cleavable Lys biotinylation reagent, EZ-Link Sulfo-NHS-SS-Biotin, at room temperature. The Western blotting is representative of three independent experiments for both *B* and *C*.

depends upon the nature of the Gly-305 substitution and whether there might be a pattern associated with a potential structural requirement. Fig. 5*A* indicates that there was little reactivation with small (Gly → Ala, Gly → Ser) substitutions, but as the Gly-305–substituted moiety became larger (Cys, Glu, Gln, Phe, Lys, and Leu), the extent of reactivation increased and was maximal irrespective of charge or polarity, with the greatest degree of restoration of activity for the G305L and G305K double mutants. This occurred despite the fact that the activity of the G305L mutant, alone, was far less than that of the G305L/D109A double mutant. The restoration of function was always greater at the saturating than low concentration, consistent with a greater increase in influx V_{max} than K_t. Whereas there was a higher degree of activation of the G305L and G305K double mutants, the expression of these mutants (Fig. 5*B*) at the cell surface was much lower (G305L/D109A) or barely detectable (G305K/D109A) in contrast to their strong expression in the crude membrane extract. To exclude the possibility that this decrease in expression at the cell surface was related to the method of measurement, which involved heating to release the biotinylated protein from the streptavidin beads, an alternative Lys biotinylation reagent was used that contains a disulfide bond that allows stripping the biotinylated protein from streptavidin beads at room temperature. Fig. 5*C* confirms that even when this method was employed, expression of the G305K/D109A, G305L/D109A, and G305Q/D109A mutants at the cell membrane was reduced as compared with PCFT-WT; however, it is now clear that this mirrors the change in PCFT expression in the membrane extract. Based upon the intensity of bands from three independent experiments, the plasma membrane expression of the G305L/D109A mutant was 55 ± 7% of that of PCFT-WT. Hence, when the level of expression is taken into consideration, the transport activity mediated by these double mutants is likely comparable with that of PCFT-WT.

Influx kinetics associated with reactivation of the D109A PCFT scaffold

[^{3}H]pemetrexed kinetics was assessed for the G305L/D109A double mutant and compared with PCFT-WT. Pemetrexed was utilized for this assay because its affinity for PCFT is much greater than that of MTX so that influx can be fully saturated even when there is a large increase in the influx K_t. It can be seen in Fig. 6 that the influx V_{max} was one-half, and that the influx K_t was 3-fold greater than, that of PCFT-WT. When the V_{max} was normalized to relative protein expression at the plasma membrane, this parameter for the G305L/D109A was even higher than that of PCFT-WT. Hence, the mobility of the double mutant was fully restored, although the affinity for pemetrexed was reduced.

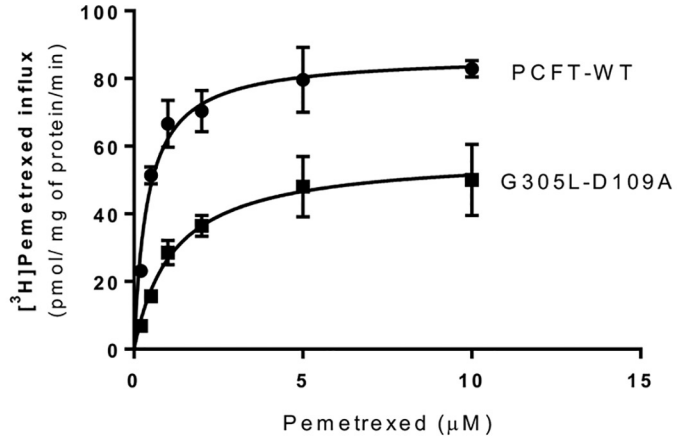

	PCFT-WT	G305L-D109A (not normalized)	G305L-D109A (normalized to surface protein level)	PCFT-WT/G305L-D109A
K_t	0.39 ± 0.08	1.15 ± 0.41	--	0.34
V_{max}	86.77 ± 4.23	57.41 ± 6.18	104.3	0.83

Figure 6. Influx kinetics associated with the restoration of function of the D109A mutant by introduction of the G305L mutation. [^{3}H]Pemetrexed (0.05–10 μM) influx kinetics was assessed at pH 5.5 for 1 min in cells transfected with either PCFT-WT or the D109A/G305L PCFT mutant. The data are best fit to the Michaelis–Menten equation, $V = V_{max}[S]/(K_t + [S])$, where V_{max} is the maximum transport rate, [S] is extracellular substrate concentration, and K_t is the concentration at which influx is one-half of maximum. Data are the mean ± S.E. (*error bars*) from three independent experiments. The V_{max} of the D109A/G305L mutant is also shown normalized to the relative expression at the plasma membrane 0.55 as compared with PCFT-WT.

Impact of the G305L mutation on the G112K loop mutant

As indicated earlier, another fully conserved residue in the first intracellular loop, Gly-112, is also required for function. Studies were undertaken to determine whether introduction of the G305L mutation into the G112K-inactivating scaffold would restore the activity of the double mutant. The D109A single and double mutants were included for the purpose of comparison. It can be seen in Fig. 7*A*, that MTX influx in the cells harboring the G112K mutation was absent, as was the case with the D109A mutant. However, the G305L/G112K double mutant was active at a level comparable with G305L-D109A ($p = 0.07$ at the high concentration and $p < 0.01$ at the low concentration as compared with the single G112K mutant). When the decrease in expression at the cell membrane and crude membrane extract are considered (Fig. 7*B*), the intrinsic activity of both mutants is even higher.

Impact of the G305L mutation on the function and cysteine accessibility of the P314C/D109A mutant

As indicated above (Fig. 4*B*), the P314C mutation that alone markedly enhances transport was abolished when introduced in the D109A scaffold. However, when the G305L mutation was introduced, there was a marked restoration of activity of the triple mutant to a level ~80% that of PCFT-WT at high substrate concentration (Fig. 8*A*). This partial restoration of activity was accompanied by partial restoration of accessibility of the P314C residue to MTSEA-biotin within this scaffold, consistent with at least partial reopening of the aqueous pathway (Fig. 8*B*).

Homology model of PCFT and identification of a second reactivating PCFT mutation

Fig. 9*A* indicates the location of the Gly-305 and Asp-109 residues within PCFT in the inward-open conformation based upon the crystal structure of the bovine GLUT5 transporter (26). The model was queried to determine whether there might be another residue in the vicinity of Gly-305 that might also reactivate the D109A mutant. Because of the rotation of the helix, no other residue in the eighth TMD produced a similar projection into the aqueous channel in either conformation. On the other hand, Gly-305 appeared to be in close proximity to Ser-196 in the fifth TMD, as seen in a planar view (Fig. 9*A*) or viewed into the transporter (Fig. 9*B*). This raised the possibility that mutations at Ser-196 might reactivate the D109A mutant protein. This turned out to be the case, as illustrated in Fig. 9*C*; when S196L or S196F mutations were introduced in the D109A scaffold, there was a small but significant reactivation of function. It can be seen that nonglycosylated forms of these mutants were present in the crude membrane extract, and the level of expression at the cell membrane was much lower than that of PCFT-WT. Hence, when the decreased level of expression is

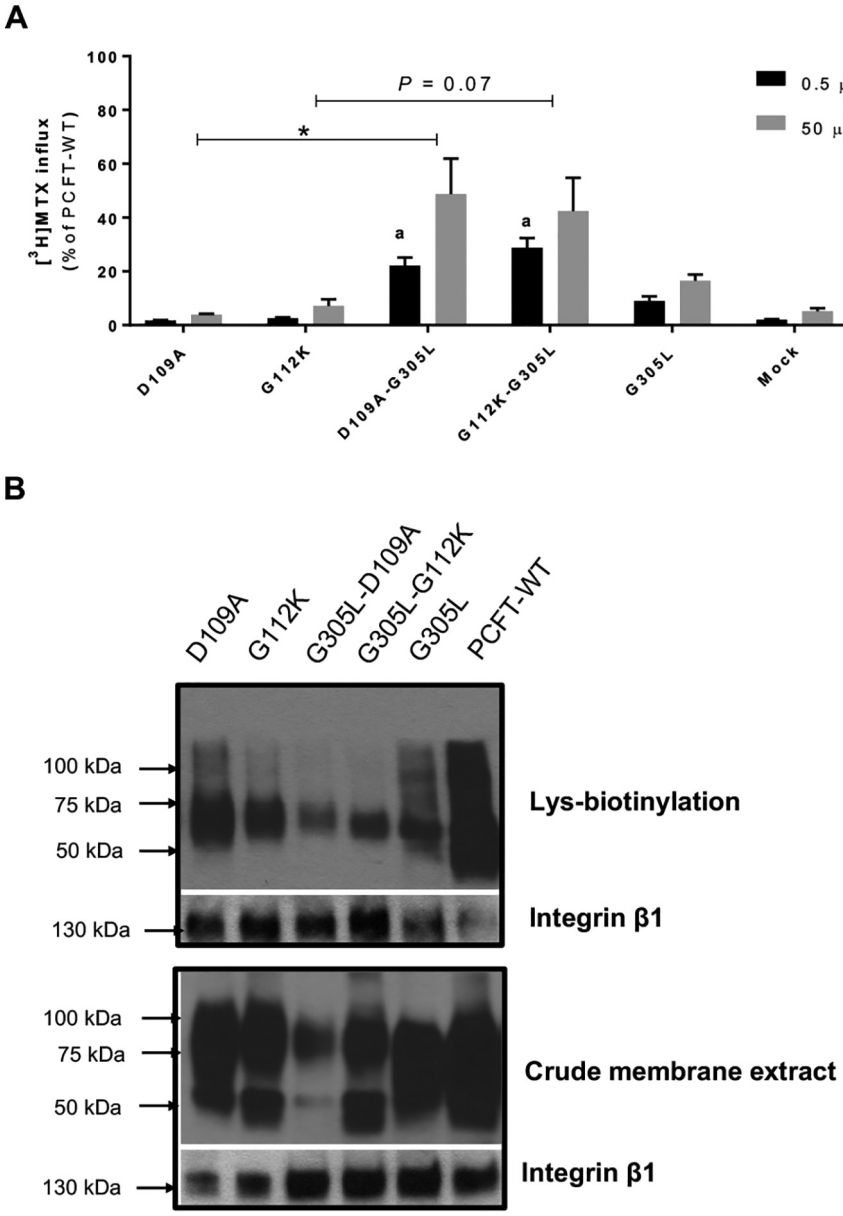

Figure 7. Impact of the introduction of the G305L mutation into the G112K and D109A scaffolds. *A*, [^{3}H]MTX influx was assessed over 1 min at pH 5.5 and 37 °C at concentrations of 0.5 and 50 μM. Data are represented as percentage ± S.E. (*error bars*) of PCFT-WT from three independent experiments. A one-way ANOVA compared D109A or G112K with their respective G305L double mutants. *, $p < 0.05$. An analysis also compared G112K/G305L with the G112K single mutant at the low concentration indicated as *a*; $p < 0.01$. *B*, in this Western blotting, PCFT expression at the cell surface is indicated in the *top row*, and expression in the crude membrane extract is indicated in the *bottom row*, each with integrin β1 as the loading control. The blot is representative of three independent experiments.

considered, the S196L or S196F mutations produced a substantial restoration of function of the D109A mutant.

Discussion

There has been considerable interest in the role that the first intracellular loop plays in PCFT function (14, 17, 27). The data in this paper indicate that the integrity of this loop is critical to the oscillation of the carrier among its conformational states and that mutations at the Asp-109 residue abolish the mobility of the protein completely while preserving expression of the protein and its trafficking to the cell membrane. The data suggest further that this loss of function occurs when this residue is replaced because the protein becomes locked in its inward open conformation. This is supported by the observations that (i) the D109A mutation results in the loss of accessibility of multiple Cys-substituted residues, including two in the region of the extracellular gate, that are accessible in PCFT-WT and that (ii) in this locked conformation, the deep cleft that forms the aqueous pathway, involving the seventh and eighth TMDs, is occluded. Unlike modifications of other residues in this transporter, transport activity of the Asp-109 mutants cannot be preserved at all even with very conservative substituting residues, including glutamate or asparagine (14).

The G*XXX*D*XX*GR(R/K) sequence that defines this region of the PCFT protein corresponds to motif A, found within the cytoplasmic loop between the second and third TMDs in other

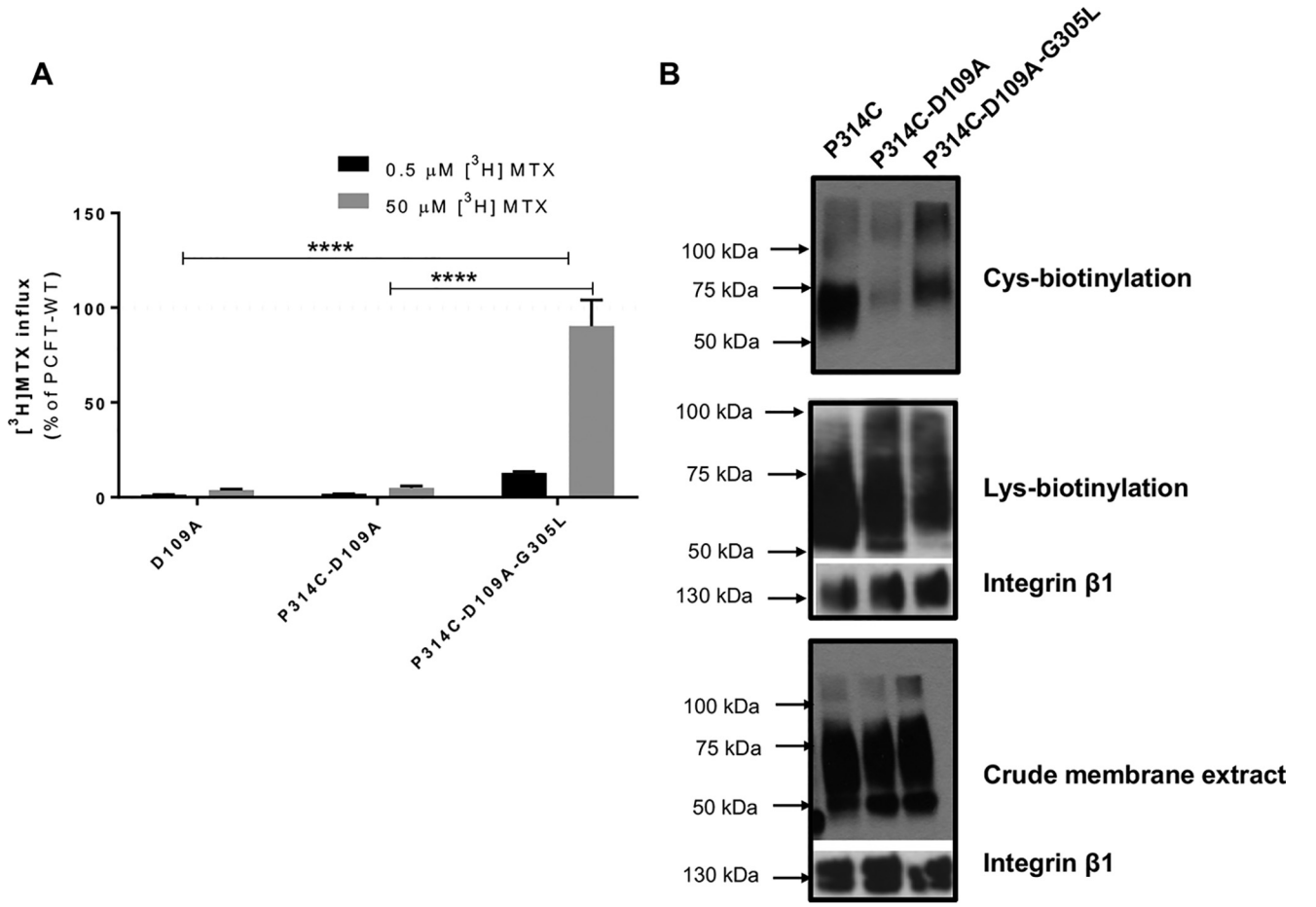

Figure 8. Impact of the introduction of the G305L mutation into the P314C-D109A scaffold and the accessibility of the P314C residue to MTSEA-biotin. *A*, [^{3}H]MTX influx was assessed at 37 °C and pH 5.5 over 1 min at concentrations of 0.5 and 50 μM. Data are represented as percentage ± S.E. of PCFT-WT influx from three independent experiments. A one-way ANOVA compared the D109A or D109A/P314C mutants with the triple mutant, D109A/P314C/G305L. ****, $p < 0.0001$. *B*, in this Western blotting, the *top panel* indicates the MTSEA-biotinylated protein, the *middle panel* shows the Lys-biotinylated protein assessed with EZ-Link Sulfo-NHS-LC, and the *bottom panel* is PCFT in the crude membrane extract. Integrin β1 serves a loading control for both the Lys-biotinylated and crude membrane proteins. The images are representative of three independent experiments.

MFS transporters (18, 19). Like PCFT, even highly conservative substitutions at the Asp residue of the lactose permease (LacY) and the metal-tetracycline/H antiporter within this loop resulted in markedly impaired function (19, 28). On the other hand, the requirement for the PCFT Gly-112 residue is more stringent than its counterpart in the LacY transporter (19). The early observation that this motif is found among MFS members that transport a variety of structurally dissimilar substrates suggested that this region is required for the interconversion of the protein between its inward- and outward- open conformations rather than playing a role in substrate binding (19).

Of particular interest was the observation that mutations at Gly-305 restored function ("suppressed" the phenotype) of the inactive D109A mutant and that the most complete restoration of function required substitutions with bulky residues independent of charge or polarity as observed for other "suppressor" mutations in other transporters (29–31). Hence, Ala and Ser substitutions did not restore function, but marked restoration of function was achieved with Leu or Lys substitutions. The first intracellular loop is located in the N-terminal half of the PCFT protein, and the Gly-305 residue is located in the carboxyl-half of the protein at the exofacial interface. The topology of this transporter (22) and the homology model of PCFT indicate that these regions of the carrier are remote (Figs. 1 and 9, respectively). Hence, it is unlikely that the restoration of function and accessibility associated with Gly-305 mutations is due to direct interactions between the G305L and D109A or G112K residues. The possibility was raised that the first intracellular loop might become extracellularly accessible, "re-entrant," during the transport cycle (17). However, subsequent studies established that Cys-substituted residues within this loop do not become accessible to extracellular sulfhydryl reagents during transitions of the protein among its conformational states (27, 32).

The restoration of function observed with substitutions at the Gly-305 residue was fortuitous. However, using selection strategies, a variety of "suppressor" mutations in diverse regions of MFS transporters were identified that restored function of proteins containing mutations at the Asp and other residues within this and related motifs (29–31). The observation that the restoration of function was associated primarily with an increase in the maximum rate of transport rather than a change in affinity for its transport substrate was considered further evidence for the critical role of this region as a determinant of the conformational changes of the protein (30, 31). With the

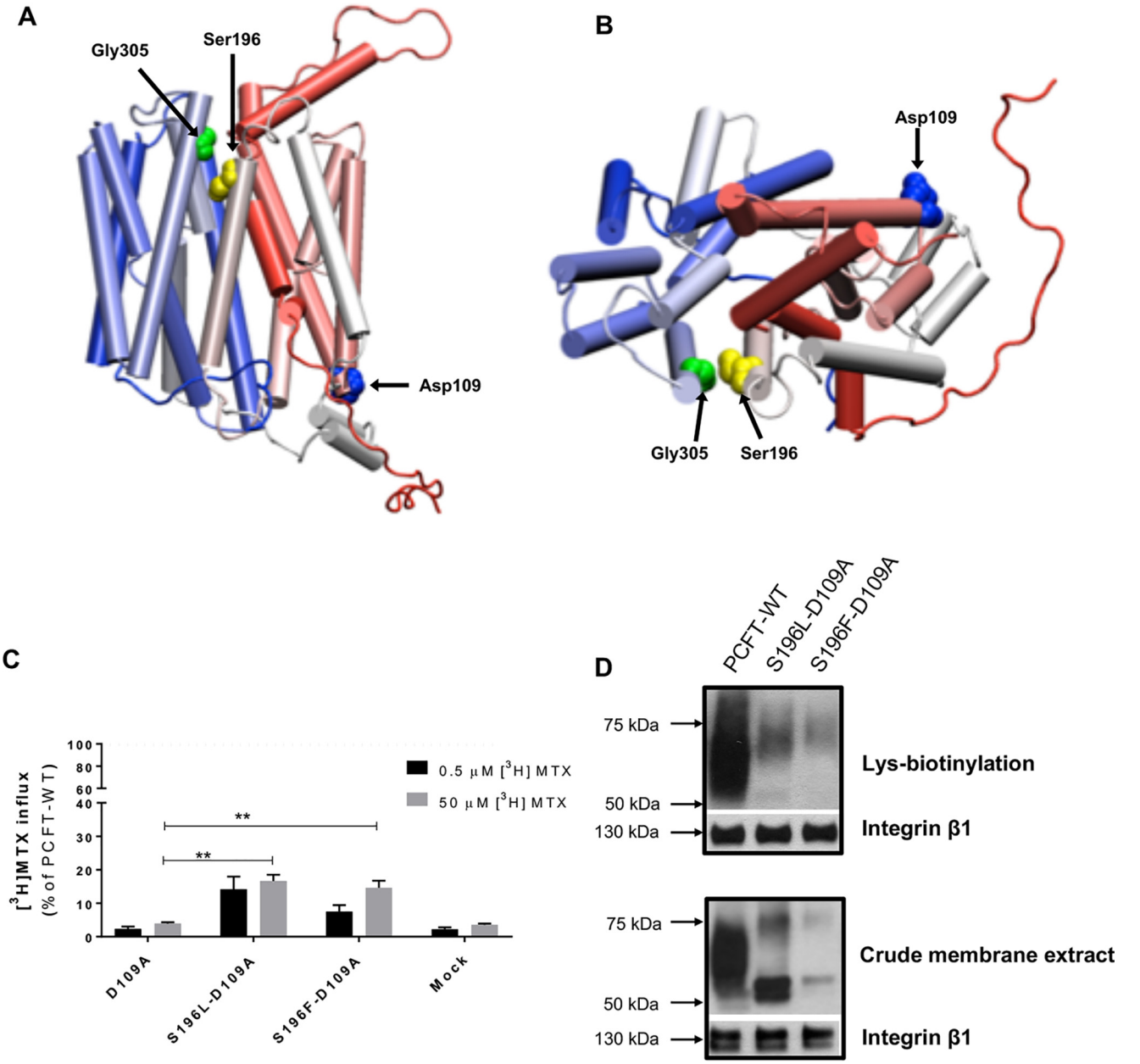

Figure 9. A homology model of PCFT depicting the locations of the Asp-109, Gly-305, and Ser-196 residues. *A*, a planar view of PCFT. *B*, a view into the protein from the extracellular compartment. The Asp-109 residue is indicated in *blue*, the Gly-305 residue in *green*, and the Ser-196 residue in *yellow*. *C*, [^{3}H]MTX influx was assessed at 37 °C over 1 min at pH 5.5 at concentrations of 0.5 and 50 μM in cells harboring the D109A mutation alone or in combination with the S196L or S196F mutation. Data are percentage ± S.E. (*error bars*) of PCFT-WT from three independent experiments. A one-way ANOVA compared D109A with the corresponding double mutants. **, $p < 0.01$. *D*, PCFT expression at the cell surface assessed with EZ-Link Sulfo-NHS-SS-Biotin is indicated in the *top panel*, and expression in the crude membrane extract is indicated in the *bottom panel*, each with integrin β1 as the loading control. The images are representative of three independent experiments.

more recent structural characterization of MFS transporters, there is further evidence for a role for motif A in stabilizing the outward conformation favoring the inward-open conformation when this this loop is disrupted (33, 34). Restoration of function by second mutations has also been observed with loss-of-function mutations in regions other than the loop between the second and third TMDs. For instance, the loss of function induced by a D389N mutation in a conserved D*XXX*R region within the eighth TMD of the LdNT2 *Leischmania donovani* nucleoside transporter was reactivated by a second bulky N175I substitution predicted to be located in close proximity within a three-dimensional model (35).

The mechanism by which Gly-305 mutations restore activity is unclear, but one possible explanation is that mutations in the first intracellular loop result in a latchlike interaction among the helices. Substitutions at the Gly-305 position may have a wedgelike effect that prevents or markedly impairs the formation of the latch. The fact that this effect is size-related supports this concept. The data indicate further that substitutions at the Ser-196 residue of the fifth TMD, which is predicted to be in close proximity to Gly-305 in the inward-open conformation, results in a similar reactivation of the protein.

There has been considerable interest in the development of techniques that "lock" solute transporters in one conformation

to eliminate oscillation of the protein in detergent solutions that impedes the formation of crystals required for structural analyses. A number of approaches have been reported. For instance, the structural characterization of hGLUT1 (36) utilized a protein with an E329Q mutation in the loop between the eighth and ninth TMDs that appeared to lock the protein in an inward-open conformation, as assessed by ATB-BMPA photolabeling and cytochalasin B binding. The rat GLUT5 transporter was crystallized in a complex with an Fv antibody fragment that stabilized the protein in an outward-open conformation. On the other hand, the unmodified bovine GLUT5 transporter could be crystallized in the inward-open conformation (26). The selection of thermostable mutants that improve stability in detergents has been another approach (37, 38). The *Drosophila* dopamine transporter structure in the outward-open conformation was obtained with several point mutations that each enhanced the protein's thermal stability with nortriptyline lodged in the central binding site (39). Likewise, thermostabilizing mutations in the human serotonin transporter and the insertion of an inhibitor into its central binding site resulted in a crystal structure in the outward-open conformation (40). In bacteria, a G45R mutation in the Nramp divalent metal transporter crystal obtained from *Dienococcus radiodurance* locked the transporter in an inward-open conformation (41). Hence, the D109A PCFT mutant may be a favorable candidate for crystallization and structural characterization.

Several of the Cys-substituted mutants studied (I188C, I287C, and P314C) exhibited a transport phenotype consistent with what has been observed for a variety of other mutants characterized in this laboratory (23, 24). These mutations that increase the influx V_{max} are invariably accompanied by an increase in the influx K_t, suggesting that these residues maintain the PCFT-WT protein in a high-affinity state for its folate substrates, which, in turn, constrains the mobility of the carrier. When these residues are mutated, flexibility increases, relaxing the protein and thereby reducing the affinity for its folate substrates. Similar kinetic changes were observed with gain-of-function mutations in the *Pyrococuccus horikoshii* glutamate transporter (42). Based upon subsequent structural analyses, this property was attributed to a direct correlation between the transport domain movements and substrate transport, suggesting an inverse relationship between substrate affinity and transport domain motions (43).

Experimental procedures

Chemicals

[3-,5-,7-^{3}H]MTX and [^{3}H]pemetrexed were purchased from Moravek Biochemicals (Brea, CA). Unlabeled methotrexate and pemetrexed were purchased from Sigma and LC Laboratories (Woburn, MA), respectively. MTSEA-biotin was purchased from Biotium (Hayward, CA). EZ-Link Sulfo-NHS-LC biotin (sulfosuccinimidyl-6-(biotinamido) hexanoate), EZ-Link Sulfo-NHS-SS-Biotin (sulfosuccinimidyl-2-[biotinamido]ethyl-1,3-dithiopropionate), and streptavidin-agarose beads were purchased from Thermo Fisher Scientific. Protease inhibitor mixture was obtained from Roche Applied Science (Mannheim, Germany).

Site-directed mutagenesis

Amino acid substitutions were generated on a PCFT-WT template using the QuikChange II XL site-directed mutagenesis kit (Stratagene, La Jolla, CA). The PCFT-WT template was cloned in pcDNA3.1(+) with a C terminus HA (hemagglutinin) tag. The ORF of all PCFT mutants was verified by sequencing at the Albert Einstein Cancer Center Genomics Facility.

Cell lines, culture, and transfection conditions

A HeLa-derived cell line, HeLa R1-11, was utilized as the transfection recipient for these experiments. This cell line lacks constitutive PCFT and RFC expression due to silencing of the promoter of the former and genomic deletion of the latter (44, 45). The cells were maintained in RPMI 1640 medium supplemented with 10% fetal bovine serum (Gemini Bio-Products, Irvine, CA), 100 units/ml penicillin, and 100 μg of streptomycin and grown as a monolayer on tissue culture plates. Three hundred thousand cells were seeded in 17-mm, 20-ml screw-topped glass vials (RPI Research Products, Mt. Prospect, IL) for transport measurements, and 5×10^5 cells/well were seeded in 6-well plates for Western blotting analyses. Forty-eight hours later, the cells were transfected with 0.8 μg of DNA/vial for transport measurements and 1.6 μg of DNA/well for Western blot analysis using Lipofectamine 2000 (Thermo Fisher Scientific).

Transport measurements

Two days after transfection, influx of either [^{3}H]MTX or [^{3}H]pemetrexed was assessed (4). The medium in the vials was aspirated, and the cells were washed twice with HBS buffer (20 mM Hepes, 140 mM NaCl, 5 mM KCl, 2 mM $MgCl_2$, and 5 mM dextrose, pH 7.4) at room temperature. The cells were then incubated in HBS at 37 °C for 20 min, the buffer was aspirated, and 0.5 ml of prewarmed MBS buffer (20 mM MES, 140 mM NaCl, 5 mM KCl, 2 mM $MgCl_2$, and 5 mM dextrose, pH 5.5) containing tritiated radiolabeled substrate was added. After 1 min, uptake was halted by the addition of 5 ml of ice-cold HBS buffer, and the cells were washed three times with HBS. The cells were then digested by the addition of 0.5 ml of 0.2 N NaOH and incubation at 65 °C for 1 h. Four hundred microliters of the digested sample was counted on a liquid scintillation spectrometer, and 20 μl was assayed for protein by the bicinchoninic acid assay (Thermo Fisher Scientific). Substrate influx is expressed as a percentage of PCFT-WT or pmol per mg of protein per min.

Analysis of surface protein expression and biotinylation of Cys-substituted residues

PCFT surface expression was assessed by biotinylation of extracellularly accessible lysine residues with EZ-Link Sulfo-NHS-LC-Biotin in most cases or EZ-Link Sulfo-NHS-SS-Biotin when specified. Accessibility of Cys-substituted residues was assessed with MTSEA-biotin. All three reagents are membrane-impermeable. Briefly, cells were washed twice with HBS (pH 7.4), followed by treatment with 0.8 mM EZ-Link Sulfo-

NHS-LC, 0.8 mM EZ-Link Sulfo-NHS-SS-Biotin, or 0.5 mM MTSEA-biotin in 1 ml of HBS buffer at room temperature for 30 min. The cells were then washed twice with HBS and 0.7 ml of hypotonic buffer (0.5 mM $NaHPO_4$ and 0.1 mM EDTA, pH 7.0) containing protease inhibitor mixture. The cells were then scraped off the plates using a cell lifter and transferred into an Eppendorf vial, followed by centrifugation at 16,000 × *g* at 4 °C for 10 min. The supernatant was aspirated, and the pellet was resuspended in 400 μl of lysis buffer (150 mM NaCl, 50 mM Tris, 1% Nonidet P-40, 0.5% sodium deoxycholate, pH 7.4); 50 μl of the suspension was added to an equal volume of 2× Laemmli buffer for analysis of PCFT expression in the crude membrane extract. The remaining 350 μl was rotated on a Rotamix for 1 h at 4 °C followed by centrifugation at 16,000 × *g* at 4 °C for 10 min. The supernatant was mixed with streptavidin-agarose beads (50 μl), prewashed with the lysis buffer, and rotated overnight on a Rotamix at 4 °C. The next day, the beads were washed twice with 0.5 ml of lysis buffer and twice with 0.5 ml in lysis buffer containing 2% SDS. Laemmli buffer (2×, with 0.2 M DTT) was added to the washed beads, mixed for 15 min at room temperature for EZ-Link Sulfo-NHS-SS-Biotin or heated at 100 °C for 5 min for EZ-Link Sulfo-NHS-LC, and then spun down at 16,000 × *g* for 2 min. The supernatant was collected and stored at −20 °C.

Gel electrophoresis and Western blot analysis

The protein samples were resolved on 4–12% polyacrylamide gels (Bio-Rad), followed by electroblotting onto polyvinylidine difluoride membranes (Millipore). The membranes were blocked with 10% nonfat milk in TBST (20 mM Tris, 135 mM NaCl, and 0.1% Tween 20 buffered to pH 7.4) and probed either with anti-HA primary antibody (catalog no. 6908, Sigma) for 90 min or anti-integrin β1 (catalog no. 9699, Cell Signaling Technology, Danvers, MA) followed by 1 h with horseradish peroxidase–conjugated secondary antibody (Cell Signaling Technology, Danvers, MA). Blots were developed with ECL Plus reagent (PerkinElmer Life Sciences).

Homology modeling

Homology modeling has been utilized to understand the structural basis for PCFT function. Recently, the structures of several mammalian solute transporters have been obtained so that it has become possible to model human PCFT with other mammalian transporters in more than one conformation. We recently reported on homology models of PCFT (13, 23) based upon structures of the bovine and rat GLUT5 fructose transporters (26) in the inward-open and outward-open conformations (Protein Data Bank codes 4YB9 and 4YBQ, respectively). These two GLUT5 transporters share 88% sequence identity with each other and 13% sequence identity to PCFT, similar to the level of identity between PCFT and GlpT (10, 16). Briefly, the optimal alignment between PCFT and the GLUT5 template structures and the subsequent molecular model was obtained from MMM alignment optimization and comparative modeling (46–48). The quality of the model was verified through energetic analysis using statistical pair potentials implemented in Pros (49). Optimal superposition of the two models was obtained using the Align3D program of Modeler (50).

Statistical analysis

Statistical analyses were performed with GraphPad Prism version 7 applying the one-way ANOVA using Fisher's least significant difference test. MTX influx at the saturation concentration (50 μM) was used for most statistical analyses due to its higher activity for each mutant relative to influx at the low concentration (0.5 μM).

Author contributions—S. A., R. Z., A. F., and I. D. G. designed the study. S. A., K. L., D. S. S., A. F., and R. Z. performed experiments. S. A., R. Z., K. L., A. F., and I. D. G. analyzed the data. S. A., R. Z., A. F., and I. D. G. wrote the paper. All of the authors contributed to and approved the final version of the paper.

References

1. Zhao, R., Aluri, S., and Goldman, I. D. (2017) The proton-coupled folate transporter (PCFT-SLC46A1) and the syndrome of systemic and cerebral folate deficiency of infancy: Hereditary folate malabsorption. *Mol. Aspects Med.* **53,** 57–72 CrossRef Medline
2. Qiu, A., Jansen, M., Sakaris, A., Min, S. H., Chattopadhyay, S., Tsai, E., Sandoval, C., Zhao, R., Akabas, M. H., and Goldman, I. D. (2006) Identification of an intestinal folate transporter and the molecular basis for hereditary folate malabsorption. *Cell* **127,** 917–928 CrossRef Medline
3. Visentin, M., Diop-Bove, N., Zhao, R., and Goldman, I. D. (2014) The intestinal absorption of folates. *Annu. Rev. Physiol.* **76,** 251–274 CrossRef Medline
4. Zhao, R., Qiu, A., Tsai, E., Jansen, M., Akabas, M. H., and Goldman, I. D. (2008) The proton-coupled folate transporter (PCFT): impact on pemetrexed transport and on antifolate activities as compared to the reduced folate carrier. *Mol. Pharmacol.* **74,** 854–862 CrossRef Medline
5. Matherly, L. H., Hou, Z., and Gangjee, A. (2018) The promise and challenges of exploiting the proton-coupled folate transporter for selective therapeutic targeting of cancer. *Cancer Chemother. Pharmacol.* **81,** 1–15 CrossRef Medline
6. Matherly, L. H., Wilson, M. R., and Hou, Z. (2014) The major facilitative folate transporters solute carrier 19A1 and solute carrier 46A1: biology and role in antifolate chemotherapy of cancer. *Drug Metab. Dispos.* **42,** 632–649 CrossRef Medline
7. Giovannetti, E., Zucali, P. A., Assaraf, Y. G., Funel, N., Gemelli, M., Stark, M., Thunnissen, E., Hou, Z., Muller, I. B., Struys, E. A., Perrino, M., Jansen, G., Matherly, L. H., and Peters, G. J. (2017) Role of proton-coupled folate transporter in pemetrexed resistance of mesothelioma: clinical evidence and new pharmacological tools. *Ann. Oncol.* **28,** 2725–2732 CrossRef Medline
8. Unal, E. S., Zhao, R., and Goldman, I. D. (2009) Role of the glutamate 185 residue in proton translocation mediated by the proton-coupled folate transporter SLC46A1. *Am. J. Physiol. Cell Physiol.* **297,** C66–C74 CrossRef Medline
9. Unal, E. S., Zhao, R., Chang, M. H., Fiser, A., Romero, M. F., and Goldman, I. D. (2009) The functional roles of the His^{247} and His^{281} residues in folate and proton translocation mediated by the human proton-coupled folate transporter SLC46A1. *J. Biol. Chem.* **284,** 17846–17857 CrossRef Medline
10. Zhao, R., Najmi, M., Fiser, A., and Goldman, I. D. (2016) Identification of an extracellular gate for the proton-coupled folate transporter (SLC46A1) by cysteine cross-linking. *J. Biol. Chem.* **291,** 8162–8172 CrossRef Medline
11. Shin, D. S., Zhao, R., Yap, E. H., Fiser, A., and Goldman, I. D. (2012) A P425R mutation of the proton-coupled folate transporter causing hereditary folate malabsorption produces a highly selective alteration in folate binding. *Am. J. Physiol. Cell Physiol.* **302,** C1405–C1412 CrossRef Medline
12. Mahadeo, K., Diop-Bove, N., Shin, D., Unal, E. S., Teo, J., Zhao, R., Chang, M. H., Fulterer, A., Romero, M. F., and Goldman, I. D. (2010) Properties of the Arg376 residue of the proton-coupled folate transporter (PCFT-SLC46A1) and a glutamine mutant causing hereditary

folate malabsorption. *Am. J. Physiol. Cell Physiol.* **299,** C1153–C1161 CrossRef Medline

13. Aluri, S., Zhao, R., Lubout, C., Goorden, S. M. I., Fiser, A., and Goldman, I. D. (2018) Hereditary folate malabsorption due to a mutation in the external gate of the proton-coupled folate transporter-SLC46A1. *Blood Adv.* **2,** 61–68 CrossRef Medline
14. Shin, D. S., Min, S. H., Russell, L., Zhao, R., Fiser, A., and Goldman, I. D. (2010) Functional roles of aspartate residues of the proton-coupled folate transporter (PCFT; SLC46A1); a D156Y mutation causing hereditary folate malabsorption. *Blood* **116,** 5162–5169 CrossRef Medline
15. Zhao, R., Min, S. H., Qiu, A., Sakaris, A., Goldberg, G. L., Sandoval, C., Malatack, J. J., Rosenblatt, D. S., and Goldman, I. D. (2007) The spectrum of mutations in the PCFT gene, coding for an intestinal folate transporter, that are the basis for hereditary folate malabsorption. *Blood* **110,** 1147–1152 CrossRef Medline
16. Lasry, I., Berman, B., Straussberg, R., Sofer, Y., Bessler, H., Sharkia, M., Glaser, F., Jansen, G., Drori, S., and Assaraf, Y. G. (2008) A novel loss of function mutation in the proton-coupled folate transporter from a patient with hereditary folate malabsorption reveals that Arg 113 is crucial for function. *Blood* **112,** 2055–2061 CrossRef Medline
17. Wilson, M. R., Hou, Z., and Matherly, L. H. (2014) Substituted cysteine accessibility reveals a novel transmembrane 2–3 reentrant loop and functional role for transmembrane domain 2 in the human proton-coupled folate transporter. *J. Biol. Chem.* **289,** 25287–25295 CrossRef Medline
18. Griffith, J. K., Baker, M. E., Rouch, D. A., Page, M. G., Skurray, R. A., Paulsen, I. T., Chater, K. F., Baldwin, S. A., and Henderson, P. J. (1992) Membrane transport proteins: implications of sequence comparisons. *Curr. Opin. Cell Biol.* **4,** 684–695 CrossRef Medline
19. Jessen-Marshall, A. E., Paul, N. J., and Brooker, R. J. (1995) The conserved motif, G*XXX*(D/E)(R/K)*X*G[*X*](R/K)(R/K), in hydrophilic loop 2/3 of the lactose permease. *J. Biol. Chem.* **270,** 16251–16257 CrossRef Medline
20. Shin, D. S., Zhao, R., Fiser, A., and Goldman, I. D. (2013) Role of the fourth transmembrane domain in proton-coupled folate transporter function as assessed by the substituted cysteine accessibility method. *Am. J. Physiol. Cell Physiol.* **304,** C1159–C1167 CrossRef Medline
21. Zhao, R., Shin, D. S., Fiser, A., and Goldman, I. D. (2012) Identification of a functionally critical G*XX*G motif and its relationship to the folate binding site of the proton-coupled folate transporter (PCFT-SLC46A1). *Am. J. Physiol. Cell Physiol.* **303,** C673–C681 CrossRef Medline
22. Zhao, R., Unal, E. S., Shin, D. S., and Goldman, I. D. (2010) Membrane topological analysis of the proton-coupled folate transporter (PCFT-SLC46A1) by the substituted cysteine accessibility method. *Biochemistry* **49,** 2925–2931 CrossRef Medline
23. Aluri, S., Zhao, R., Fiser, A., and Goldman, I. D. (2017) Residues in the eighth transmembrane domain of the proton-coupled folate transporter (SLC46A1) play an important role in defining the aqueous translocation pathway and in folate substrate binding. *Biochim. Biophys. Acta Biomembr.* **1859,** 2193–2202 CrossRef Medline
24. Visentin, M., Unal, E. S., Najmi, M., Fiser, A., Zhao, R., and Goldman, I. D. (2015) Identification of Tyr residues that enhance folate substrate binding and constrain oscillation of the proton-coupled folate transporter (PCFT-SLC46A1). *Am. J. Physiol. Cell Physiol.* **308,** C631–C641 CrossRef Medline
25. Aluri, S., Zhao, R., Fiser, A., and Goldman, I. D. (2018) Substituted-cysteine accessibility and cross-linking identify an exofacial cleft in the 7th and 8th helices of the proton-coupled folate transporter (SLC46A1). *Am. J. Physiol. Cell Physiol.* **314,** C289–C296 CrossRef Medline
26. Nomura, N., Verdon, G., Kang, H. J., Shimamura, T., Nomura, Y., Sonoda, Y., Hussien, S. A., Qureshi, A. A., Coincon, M., Sato, Y., Abe, H., Nakada-Nakura, Y., Hino, T., Arakawa, T., Kusano-Arai, O., Iwanari, H., Murata, T., Kobayashi, T., Hamakubo, T., Kasahara, M., Iwata, S., and Drew, D. (2015) Structure and mechanism of the mammalian fructose transporter GLUT5. *Nature* **526,** 397–401 CrossRef Medline
27. Zhao, R., Najmi, M., Aluri, S., and Goldman, I. D. (2017) Impact of post-translational modifications of engineered cysteines on the substituted cysteine accessibility method; evidence for glutathionylation. *Am. J. Physiol. Cell Physiol.* **312,** C517–C526 CrossRef Medline
28. Yamaguchi, A., Ono, N., Akasaka, T., Noumi, T., and Sawai, T. (1990) Metal-tetracycline/H^+ antiporter of *Escherichia coli* encoded by a transposon, Tn10: The role of the conserved dipeptide, Ser^{65}-Asp^{66}, in tetracycline transport. *J. Biol. Chem.* **265,** 15525–15530 Medline
29. Yamaguchi, A., Inagaki, Y., and Sawai, T. (1995) Second-site suppressor mutations for the Asp-66 → Cys mutant of the transposon Tn10-encoded metal-tetracycline/H^+ antiporter of *Escherichia coli*. *Biochemistry* **34,** 11800–11806 CrossRef Medline
30. Jessen-Marshall, A. E., Parker, N. J., and Brooker, R. J. (1997) Suppressor analysis of mutations in the loop 2–3 motif of lactose permease: evidence that glycine-64 is an important residue for conformational changes. *J. Bacteriol.* **179,** 2616–2622 CrossRef Medline
31. Cain, S. M., Matzke, E. A., and Brooker, R. J. (2000) The conserved motif in hydrophilic loop 2/3 and loop 8/9 of the lactose permease of *Escherichia coli*: analysis of suppressor mutations. *J. Membr. Biol.* **176,** 159–168 CrossRef Medline
32. Date, S. S., Chen, C. Y., Chen, Y., and Jansen, M. (2016) Experimentally optimized threading structure of the proton-coupled folate transporter. *FEBS Open Bio* **6,** 216–230 CrossRef Medline
33. Liu, Z., Madej, M. G., and Kaback, H. R. (2010) Helix dynamics in LacY: helices II and IV. *J. Mol. Biol.* **396,** 617–626 CrossRef Medline
34. Jiang, D., Zhao, Y., Wang, X., Fan, J., Heng, J., Liu, X., Feng, W., Kang, X., Huang, B., Liu, J., and Zhang, X. C. (2013) Structure of the YajR transporter suggests a transport mechanism based on the conserved motif A. *Proc. Natl. Acad. Sci. U.S.A.* **110,** 14664–14669 CrossRef Medline
35. Arastu-Kapur, S., Arendt, C. S., Purnat, T., Carter, N. S., and Ullman, B. (2005) Second-site suppression of a nonfunctional mutation within the *Leishmania donovani* inosine-guanosine transporter. *J. Biol. Chem.* **280,** 2213–2219 CrossRef Medline
36. Deng, D., Xu, C., Sun, P., Wu, J., Yan, C., Hu, M., and Yan, N. (2014) Crystal structure of the human glucose transporter GLUT1. *Nature* **510,** 121–125 CrossRef Medline
37. Serrano-Vega, M. J., Magnani, F., Shibata, Y., and Tate, C. G. (2008) Conformational thermostabilization of the β1-adrenergic receptor in a detergent-resistant form. *Proc. Natl. Acad. Sci. U.S.A.* **105,** 877–882 CrossRef Medline
38. Magnani, F., Serrano-Vega, M. J., Shibata, Y., Abdul-Hussein, S., Lebon, G., Miller-Gallacher, J., Singhal, A., Strege, A., Thomas, J. A., and Tate, C. G. (2016) A mutagenesis and screening strategy to generate optimally thermostabilized membrane proteins for structural studies. *Nat. Protoc.* **11,** 1554–1571 CrossRef Medline
39. Penmatsa, A., Wang, K. H., and Gouaux, E. (2013) X-ray structure of dopamine transporter elucidates antidepressant mechanism. *Nature* **503,** 85–90 CrossRef Medline
40. Coleman, J. A., Green, E. M., and Gouaux, E. (2016) X-ray structures and mechanism of the human serotonin transporter. *Nature* **532,** 334–339 CrossRef Medline
41. Bozzi, A. T., Bane, L. B., Weihofen, W. A., Singharoy, A., Guillen, E. R., Ploegh, H. L., Schulten, K., and Gaudet, R. (2016) Crystal structure and conformational change mechanism of a bacterial Nramp-family divalent metal transporter. *Structure* **24,** 2102–2114 CrossRef Medline
42. Ryan, R. M., Kortt, N. C., Sirivanta, T., and Vandenberg, R. J. (2010) The position of an arginine residue influences substrate affinity and K^+ coupling in the human glutamate transporter, EAAT1. *J. Neurochem.* **114,** 565–575 CrossRef Medline
43. Akyuz, N., Georgieva, E. R., Zhou, Z., Stolzenberg, S., Cuendet, M. A., Khelashvili, G., Altman, R. B., Terry, D. S., Freed, J. H., Weinstein, H., Boudker, O., and Blanchard, S. C. (2015) Transport domain unlocking sets the uptake rate of an aspartate transporter. *Nature* **518,** 68–73 CrossRef Medline
44. Diop-Bove, N. K., Wu, J., Zhao, R., Locker, J., and Goldman, I. D. (2009) Hypermethylation of the human proton-coupled folate transporter (SLC46A1) minimal transcriptional regulatory region in an antifolate-resistant HeLa cell line. *Mol. Cancer Ther.* **8,** 2424–2431 CrossRef Medline
45. Zhao, R., Gao, F., Hanscom, M., and Goldman, I. D. (2004) A prominent low-pH methotrexate transport activity in human solid tumor cells: contribution to the preservation of methotrexate pharmacological activity in

HeLa cells lacking the reduced folate carrier. *Clin. Cancer Res.* **10,** 718–727 CrossRef Medline

46. Fernandez-Fuentes, N., Madrid-Aliste, C. J., Rai, B. K., Fajardo, J. E., and Fiser, A. (2007) M4T: a comparative protein structure modeling server. *Nucleic Acids Res.* **35,** W363–W368 CrossRef Medline
47. Rai, B. K., Madrid-Aliste, C. J., Fajardo, J. E., and Fiser, A. (2006) MMM: a sequence-to-structure alignment protocol. *Bioinformatics* **22,** 2691–2692 CrossRef Medline
48. Rai, B. K., and Fiser, A. (2006) Multiple mapping method: a novel approach to the sequence-to-structure alignment problem in comparative protein structure modeling. *Proteins* **63,** 644–661 CrossRef Medline
49. Sippl, M. J. (1993) Recognition of errors in three-dimensional structures of proteins. *Proteins* **17,** 355–362 CrossRef Medline
50. Fiser, A., and Sali, A. (2003) Modeller: generation and refinement of homology-based protein structure models. *Methods Enzymol.* **374,** 461–491 CrossRef Medline